J Solid State Electrochem (2012) 16:2571–2579
DOI 10.1007/s10008-012-1676-9

ORIGINAL PAPER

Mass transport and kinetics of electrochemical oxygen reduction at nanostructured platinum electrode and solid polymer electrolyte membrane interface

Junhua Jiang · Anthony Kucernak

Received: 12 December 2011 / Revised: 31 January 2012 / Accepted: 2 February 2012 / Published online: 17 February 2012

Abstract Oxygen reduction reaction (*orr*) at nanostructured Pt electrode in a flooded polymer electrolyte membrane fuel cell environment has been investigated using a nanoporous Pt–Nafion membrane composite microelectrode by means of steady-state voltammetry and chronoamperometry. The interfacial mass transport of dissolved oxygen is characterized by comparable diffusion coefficients and lower concentrations as compared with literature data obtained with a humidified membrane. The exchange current densities measured at the nanoporous Pt and membrane interface are higher than those reported for the orr in acidic solutions or at polycrystalline Pt and Nafion membrane interface, indicating the improvement of the orr kinetics. Increasing temperature substantially improves the orr kinetics and accelerates the diffusion of oxygen, as expected by their Arrhenius behavior. At the nanoporous Pt and membrane interface, the *Tafel* plot exhibits an unusual slope of around 240 mV dec^{-1} at high overpotentials. This Tafel slope doubling the value of 120 mV dec^{-1} normally reported for the orr in acidic media and at the polycrystalline Pt and membrane interface is a signature of non-uniform polarization of the nanoporous Pt electrode on the membrane which origins have been discussed.

J. Jiang (✉)
Illinois Sustainable Technology Center,
University of Illinois at Urbana-Champaign,
Champaign, IL 61820, USA
e-mail: jjiang@istc.illinois.edu

A. Kucernak
Department of Chemistry, Imperial College London,
London SW7 2AZ, UK
e-mail: anthony@imperial.ac.uk

Keywords Oxygen reduction · Reaction kinetics · Nanostructured electrode · Electrode polarization · Mass transport

Introduction

Polymer electrolyte membrane fuel cells (PEMFCs) have been recently the focus of many academic and industrial investigations due to their high power density and low operation temperature, and as a result, the oxygen reduction reaction (*orr*) has received extensive attention. In order to explore the activity of various catalyst materials, to deduce their structure–activity relationships, and to elucidate the roles of electrode poisons and each component in co-catalysts, these reactions have been extensively studied on single [1–4] and multi-component [5–9] metal catalysts. In order to optimize the electrode structure or to study the influence of polymer electrolyte film on the mass transport and the reaction kinetics, the reactions have been also investigated at polymer electrolyte modified electrodes [10–12]. Recently, the preparation of nanoparticulate catalysts is one potential area which can provide the necessary technological advances to fuel cell technology [13]. Interest in the application of nanostructured catalysts results from the unique electronic structure of the nano-sized metal particles and their highly developed surface areas. This character is essential for the optimum functioning of a catalyst as the chemical reaction takes place on the surface of the particle.

To understand the kinetics of the orr on the nanostrucutured catalysts and their structure–activity relationships is therefore of urgent interests. A pronounced size effect of platinum for the orr has been disclosed [14, 15]. An optimum diameter of the catalyst particles has been suggested as about 2–3 nm. The

orr kinetics on nanosized platinum and platinum-based alloy catalysts has examined in aqueous solution with H_2SO_4 or H_3PO_4 as supporting electrolyte normally using rotating disk electrode techniques [16, 17]. However, the mass transport and the electrode kinetics of fuel cell reactions are different in PEMFCs. The presence of Nafion film enhances the orr kinetics [18, 19]. It is therefore important to study these reactions at the nanostructured catalyst/Nafion membrane interface in the absence of supporting electrolyte.

This can be achieved by using solid polymer electrolyte composite microelectrode in a solid-state electrochemical cell [20–26]. Such kind of microelectrode has the merits of conventional microelectrode and avoids the limitation of added supporting electrolyte. It has been extensively developed to study the electrochemical reactions occurring at the electrode/electrolyte membrane interface [20–24], the mass transport of reactants in the membrane [25], and the analyses of electroactive species [26]. The orr kinetics and the mass transport of oxygen in the membrane have been well studied using solid polymer electrolyte membrane composite Pt microdisk electrodes by Srinivasan et al. [20, 21] and Holdcroft et al. [23, 24].

The development of nanostructured microelectrode allows the investigation of the orr kinetics at nanostructured catalyst/Nafion membrane interface without adding supporting electrolyte. Nanostructured microelectrodes can be conveniently prepared from the aqueous domains of the lyotropic liquid crystalline phases of oligoethylene oxide nonionic surfactants containing dissolved metal compounds [27]. The nanostructured metal or alloy films with high specific surface areas and uniform pore size, which is strongly attached on the substrate microdisk, have received considerable attention due to their potential application in fuel cells [28, 29], sensors [30], supercapacitors, and batteries [31]. The electrochemically prepared nanostructured microelectrodes show high surface area while keeping the advantages of the conventional microelectrode and are an interesting technique for the study of the mass transport and kinetics of electrochemical reactions at nanostructured catalysts.

In this work, we have investigated the orr kinetics and mass transport of oxygen in the Nafion membrane in a solid polymer electrolyte fuel cell environment at varying temperatures using a nanoporous Pt–Nafion membrane composite microelectrode. At the nanoporous Pt and membrane interface, improved orr kinetics and non-uniform electrode polarization have been found.

Experimental

Chemicals and materials

The surfactant, octaethylene glycol monohexadecyl ether ($C_{16}EO_8$; 98%, Fluka), hexachloroplatinic acid hydrate (HCPA; 99.9%, Aldrich), Nafion solution (5 wt.%, Aldrich), and sulfuric acid (AnalaR grade, BDH) were used as received without further purification. All solutions were prepared from deionized water (18 MΩ cm resistivity, Millipore MilliQ system). Oxygen and argon were of high purity (99.99%, BOG Gases). As-received Nafion® 117 membrane was used in this work. The membrane was pretreated in boiling 3 vol.% peroxide hydrogen (AnalaR, BDH) for 30 min and then in boiling 0.5 mol dm^{-3} sulfuric acid for 30 min to remove impurities followed by being sonicated in deionized water. The membrane was stored under deionized water before use.

Preparation of nanostructured microelectrode

The nanoporous Pt microelectrode was deposited onto a gold microdisk electrode of 60 μm in diameter from an electroplating mixture comprising 42 wt.% $C_{16}EO_8$, 29 wt.% HCPA, and 29 wt.% water by stepping the potential from 0.80 to 0.14 V vs. a Ag/AgCl reference electrode for 1,200 s. In the following sections, this kind of Pt electrodeposited from hexagonal lyotropic liquid crystalline phase was denoted as H_I-ePt. The effective diameter of the gold substrate and the deposited H_I-ePt microdisk calculated from the diffusion-limiting current measured in 0.01 mol dm^{-3} $K_3Fe(CN)_6$+0.5 mol dm^{-3} KCl solution are 53 and 55 μm, respectively, assuming $D=7.63\times10^{-6}$ cm^2 s^{-1} [32] and $n=1$.

Characterization of nanostructured microelectrode

The electrode nanostructures were characterized using scanning electron microscope (SEM) and transmission electron microscope (TEM). The SEM images were obtained using a LEO 1525 Gemini field emission scanning electron microscope operating at 20 kV equipped with an Inca energy-dispersive X-ray spectroscope (Oxford Instruments). The TEM images were taken on a JEOL 2000FX transmission electron microscope operating at a voltage of 200 kV.

The SEM images clearly show the interesting spherical morphology of the H_I-ePt deposited from the liquid crystalline phases, Fig. 1a. The deposits consist of aggregated fine particles with a uniform size smaller than 50 nm. It is important to note that these particles are not solid, but have a nanoporous morphology. On the outer edge or top of the deposits are a few spherical particles smaller than the particles deposited further into the film. The TEM images unambiguously reveal a highly porous structure for the deposits, Fig. 1b.

The end-on view of a hexagonally closed packed array of pores can be clearly seen in the aggregated nanoparticles. White regions correspond to the deposited Pt, whereas dark spots distributed over the white regions

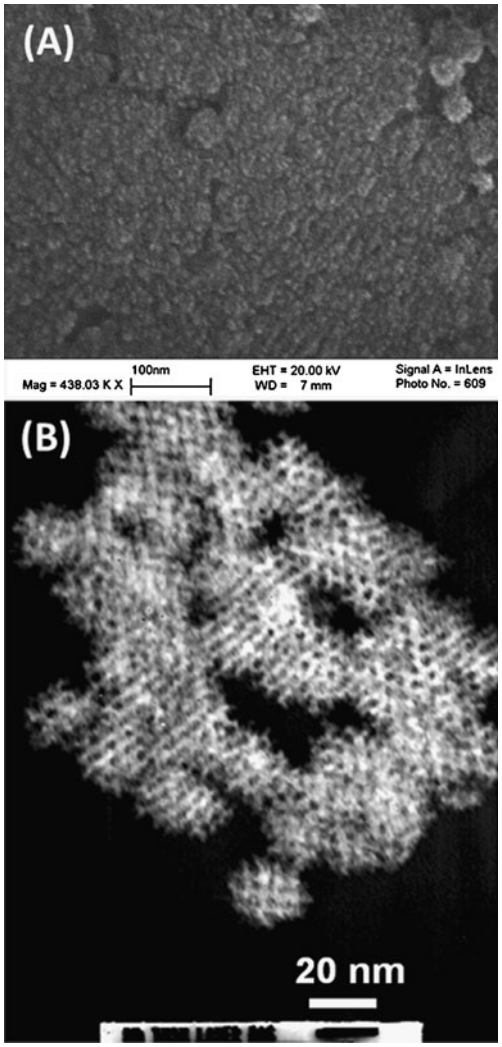

Fig. 1 SEM (**a**) and inverted TEM (**b**) images of H_I-ePt

correspond to the pores left after removal of the surfactant. The average diameters of the pores and the thickness of their walls separating them are measured to be 2.4±0.4 and 2.4±0.4 nm, respectively. These values are comparable with those found for electrodeposited nanoporous Pt film from the lyotropic liquid crystalline phases of the same surfactant [30].

Electrochemical measurements

An all-solid-state electrochemical cell was used for electrochemical measurements, which was described in our previous report [27]. Figure 2 shows a schematic diagram of the electrochemical cell for the electrochemical measurements. The working electrode compartment and the counter electrode compartment are separated by a Nafion membrane. Gases or liquids can flow separately through the two compartments. The composite microelectrode was constructed by mechanically pressing the H_I-ePt microelectrode onto the membrane

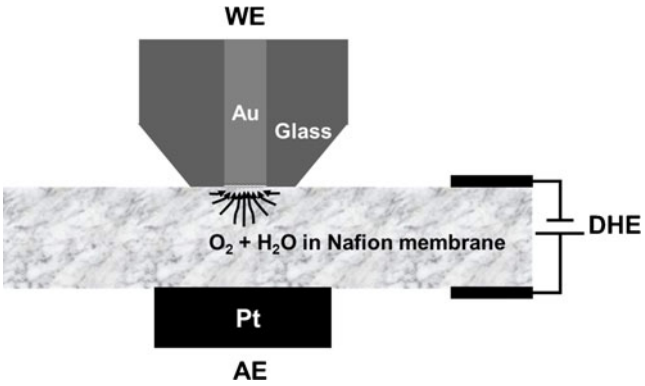

Fig. 2 A schematic diagram of an all-solid-state electrochemical cell. *WE* nanostructured H_I-ePt microelectrode, *AE* platinum plate counter electrode, *RE* dynamic hydrogen electrode (*DHE*)

supported by a platinum plate counterelectrode. A dynamic hydrogen electrode (DHE) was used as the reference electrode, consisting of two platinum plates of 0.5 cm^2 sandwiching part of the Nafion membrane. Because the overpotential for the hydrogen evolution on high-surface Pt black electrode under micro-polarization can be neglected, the DHE is reasonably approximated as the reversible hydrogen electrode (RHE) in our case. In the following sections, all potentials below were corrected to the RHE scale unless otherwise stated.

During electrochemical measurements, Ar- or O_2-saturated water was slowly pumped at 2 ml min^{-1} through the working electrode compartment using a Minipuls 3 peristaltic pump (Gilson, USA). The time taken for the system to reach a steady state, which was determined by monitoring changes in cyclic voltammograms, was about 4 h. For a given temperature increase of 20 K, the equilibrium time is about 30 min.

Both voltammetric and chronoamperometric measurements were performed using Autolab general purpose electrochemical system (Ecochemie, Netherlands). Electrochemical surface area for the nanoporous Pt/Nafion composite electrode was assessed from cyclic voltammograms obtained at a scan rate of 200 mV s^{-1}. Slow-sweep voltammograms were recorded at a scan rate of 5 mV s^{-1} to investigate the reaction kinetics and to determine the diffusion-limited current. Mass transport was further studied by chronoamperometry. In the chronoamperometric measurements, the potential of the electrode was first held at a value where no reaction occurs and then stepped to a value where the reaction is diffusion controlled.

Determination of diffusion coefficient and concentration

In our case, the chronoamperometric curves under diffusion control at the composite microelectrode could be described by following equations derived at a microdisk electrode in an ordinary cell [33].

$$I = \pi^{1/2} nFD^{1/2} c^{o} r^{2} / t^{1/2} + 4nFDc^{o} r \quad (1)$$

where n is the number of electrons transferred in the overall reaction, D the apparent diffusion coefficient, c^o the concentration, and r the radius of the microdisk. At long time, the chronoamperometric current is almost the same as the diffusion-limiting current I_d on steady-state voltammograms. At a microdisk electrode under steady-state condition, the diffusion-limited current I_d is given by [34]:

$$I_d = 4nFDc^o r \quad (2)$$

If the diffusion of the electroactive species in the membrane is not too slow or not too fast, the semi-infinite diffusion condition still holds. Moreover, the diffusion of electroactive species in the polymer electrolyte membrane is similar to that in a fluid electrolyte solution [35]. The polarization theories of a usual microdisk electrode in an ordinary cell can be applied to the solid polymer electrolyte membrane composite electrode. For a powdery microelectrode with high surface area, Eq. 2 is still valid [36]. It is reasonable to describe the diffusion-limiting current at the nanoporous H_I-ePt/Nafion composite microelectrode using Eq. 2.

Therefore, D and c^o at a given temperature can be obtained from Eqs. 3 and 4

$$D = \frac{4}{\pi^3}\left(\frac{I_d}{\delta} r\right)^2 \quad (3)$$

$$c^o = \frac{\pi^3 \delta^2}{16nFI_d r^3} \quad (4)$$

where δ is the slope of an I versus $t^{-1/2}$ plot according to Eq. 1.

Results

Electrochemical characterization of nanoporous Pt microelectrode

Figure 3 shows cyclic voltammograms for a nanoporous H_I-ePt microelectrode in 0.5 mol dm^{-3} H_2SO_4 and on the Nafion membrane at a scan rate of 200 mV s^{-1}. In an acidic solution, well-defined hydrogen and oxygen electrochemistry are observed. However, the processes associated with hydrogen and oxygen adsorption/desorption are suppressed on the membrane. The electrochemical surface area of the Pt microelectrode can be estimated from the hydrogen adsorption/desorption charge, Q_H, in the potential range of 0~0.40 V, assuming a monolayer of hydrogen corresponds to an adsorption charge of 210 μC cm^{-2}. Q_H can be determined via $Q_H = 0.5(Q_{total} - Q_{dl})$, where Q_{total} and Q_{dl} are the charge surrounded by the hydrogen adsorption/desorption curve and the capacitative charge due to double-layer charging, respectively. The electrochemical surface area of the Pt microelectrode in the acidic solution

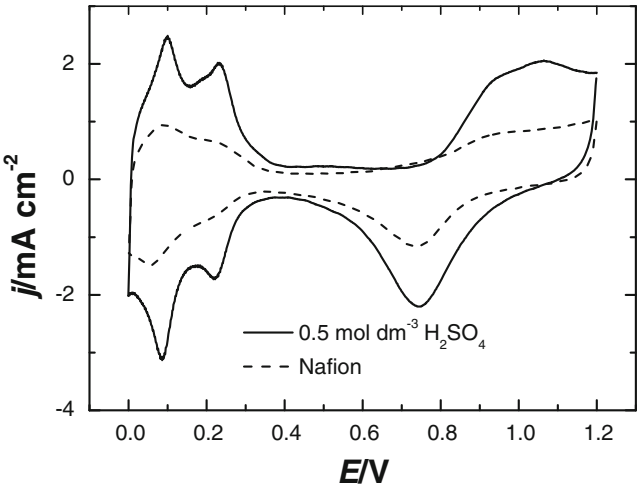

Fig. 3 Cyclic voltammograms for a H_I-ePt microelectrode in Ar-saturated 0.5 mol dm^{-3} H_2SO_4 (*solid line*) and mechanically pressed onto a Nafion membrane (*dash line*) (dE/dt, 200 mV s^{-1})

is estimated as being 3.6×10^{-4} cm^2, corresponding to an equivalent roughness factor of 15. This value is decreased to 1.5×10^{-4} cm^2 for the electrode on the membrane. These values indicate that only 42% of the electrode surface area is electrochemically active when the electrode is moved away from the acidic solution onto the membrane.

Oxygen permeation in the membrane

Steady-state polarization curves for the orr at the nanoporous Pt/Nafion interface at a given temperature are shown in Fig. 4. It is clearly seen during the negatively going scan that the diffusion-limiting current is considerably increased with increasing temperature. A substantial hysteresis occurs during the reverse scan and becomes more pronounced at higher temperature. Trace levels of organic contaminants in the

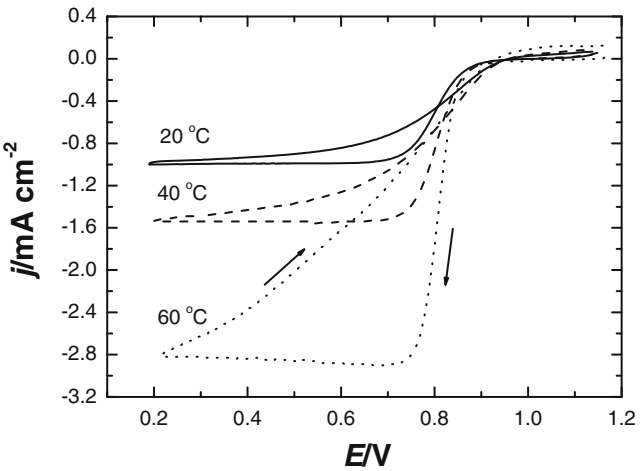

Fig. 4 Steady-state voltammograms for a H_I-ePt microelectrode/Nafion membrane equilibrated with O_2-saturated water as a function of temperature (dE/dt, 5 mV s^{-1})

Nafion membrane which block the surface at lower potentials and are oxidized at higher potentials are suggested to be responsible for this hysteresis behavior [20, 21]. This is a common feature of all attempts to make such measurements, although this problem is seldom discussed in the literature. Chronoamperometric profiles measured after stepping the potential from 1.20 to 0.25 V where the reaction is diffusion controlled as a variation of temperature are shown in Fig. 5. The inset to this figure shows linear $j \sim t^{-1/2}$ relationship.

By comparing the solubility of oxygen in water, the partition coefficient of oxygen between the membrane and water can be estimated from Henry's Law.

$$c^{o} = \aleph c_b \tag{5}$$

where c_b is the oxygen solubility in water, and $\aleph$ is the Henry's constant and is approximated as the partition coefficient.

A rough estimation of the activation energy for O_2 diffusion (E_d), the enthalpy of dissolution of O_2 in the membrane (ΔH_s), and activation energy for O_2 permeability in the membrane (E_p) can be obtained from the following equations:

$$E_d = -R\frac{d\ln D}{d(\frac{1}{T})} \tag{6}$$

$$\Delta H_s = -R\frac{d\ln c^{o}}{d(\frac{1}{T})} \tag{7}$$

$$E_p = -R\frac{d\ln(Dc^{o})}{d(\frac{1}{T})} \tag{8}$$

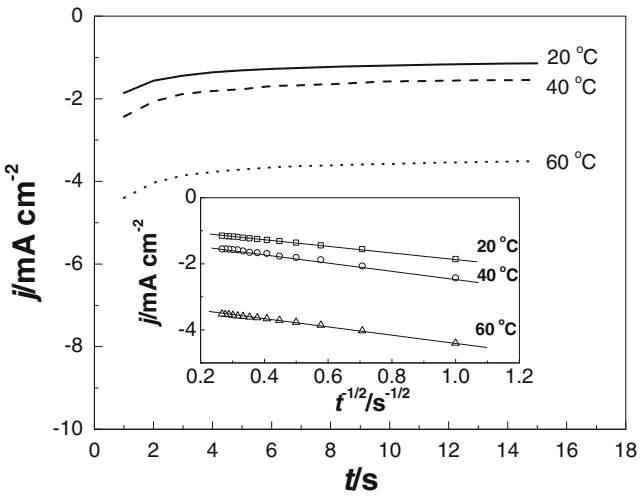

Fig. 5 Current–time transients obtained by stepping potential from 1.2 to 0.25 V for 15 s for the orr at a H_I-ePt microelectrode/Nafion membrane equilibrated with O_2-saturated water as a function of temperature. *Inset* $j \sim t^{-1/2}$ plots

Diffusion coefficient, solubility, and permeability of oxygen in a flooded Nafion membrane as a function of temperature are shown in Table 1. At room temperature, the diffusion efficient and concentration are 1.2×10^{-6} cm^2 s^{-1} and 4.5×10^{-6} mol cm^{-3}, respectively. In a flooded as-received membrane, the values of D and c^{o} were reported to be 2.4×10^{-7} cm^2 s^{-1} and 7.2×10^{-6} mol cm^{-3}, respectively [37, 38]. In a humidified membrane with 1~5 atm oxygen through the working electrode chamber, higher values of D and c^{o} are reported [20, 21, 23, 24]. The difference between our values and literature data is likely to associate with differences in water content in the membranes. Partially or fully humidified membranes can facilitate the permeation of oxygen than flooded membranes. Moreover, the maintenance of oxygen pressure in the working electrode chamber can increase the solubility of oxygen in the membrane if its dissolution follows Henry's Law [23, 24].

Table 1 shows that D is increased as temperature is increased. The trend is similar to literature results with D increasing from 1.0×10^{-6} to 6.2×10^{-6} cm^2 s^{-1} in the same temperature range but in humidified membrane and/or at different oxygen pressures [39]. The activation energy for O_2 diffusion in the flooded membrane is estimated as being 36.9±8.4 kJ mol^{-1} according to Eq. 6 by means of an Arrhenius-type plot. This value, larger than the literature data of 20.1 kJ mol^{-1} in the humidified membrane [24], indicates that increasing temperature can promote O_2 diffusion more efficiently in the flooded membrane. At 60 °C, the D value under the flooding condition is very close to that measured under the humidifying condition.

The concentration of oxygen in the flooded membrane is decreased with increasing temperature. The enthalpy of dissolution of O_2 in the membrane, ΔH_s, is approximately estimated as being −22.3±3.1 kJ mol^{-1} [24]. This value is higher than the literature value of −8.1 kJ mol^{-1} measured in the humidified membrane. According to Eq. 5, at room temperature, $\aleph$=3 is obtained from 1.40×10^{-6} mol cm^{-3} of c_b [40]. The values of $\aleph$ at varying temperature are provided in Table 1.

Table 1 Diffusion coefficients (D), solubility (c^{o}), permeability (Dc^{o}) for O_2 in a flooded Nafion membrane at a given temperature, Henry's constant ($\aleph$) and estimated diffusion activation energy (E_d), dissolution enthalpy (ΔH_s), and permeability activation energy (E_p)

Temperature/K	$10^6\times D$/ cm^2 s^{-1}	$10^6\times c^{o}$/ mol cm^{-3}	$10^{12}\times Dc^{o}$/ mol cm^{-1} s^{-1}	$\aleph$
293	1.2	4.5	5.4	3.2
313	4.5	2.2	8.6	2.5
333	7.3	1.5	16.0	1.4
E_d, ΔH_s, or E_p/ kJ mol^{-1}	36.9±8.4	−22.3±3.1	21.9±2.6	–

The permeability of oxygen in the flooded membrane shows an obvious temperature dependence. Its activation energy is determined as being 21.9±2.6 kJ mol^{-1}, higher than the value of 7.9 kJ mol^{-1} obtained in the humidified membrane [40].

Kinetics of orr

Quantitative data for the orr kinetics were obtained via mass transport corrected *Tafel* plots, Fig. 6. The plots show two pseudo-linear regions. This break in the Tafel slope seen at a potential of 0.80~0.85 V has been observed and interpreted as a change in orr mechanism [21]. The value of the low Tafel slope increases from 78 to 97 mV dec^{-1} as temperature is increased from 20 to 60 °C, while the value of the high slope changes from 232 to 300 mV dec^{-1} in the same temperature range. These values are clearly higher than reported values of *RT/F* (~60 mV dec^{-1}) at low overpotential and of *2RT/F* (~120 mV dec^{-1}) at high overpotential for the orr at Pt electrode in acidic media and at the Pt/Nafion interface [20, 24]. The unusual difference between our values and literature data may be caused by different orr kinetics at the nanoporous Pt/Nafion interface or the interference of impurities in the membrane and on the electrode surface. In order to rule out the possibility that surfactant residue from the preparation affects the orr kinetics, steady-state voltammograms for the orr on the H_I-ePt microelectrode in 0.5 mol dm^{-3} H_2SO_4 are shown in Fig. 3 and resulted Tafel plot is inset to the figure. Two normal values, 59 mV dec^{-1} at low overpotential and 100 mV dec^{-1} at high overpotential, are obtained. From the normal Tafel slopes and well-defined hydrogen electrochemistry shown in a solid line in Fig. 7, the influence of the surfactant residue on the high Tafel slope for the H_I-ePt electrode on the membrane can be neglected.

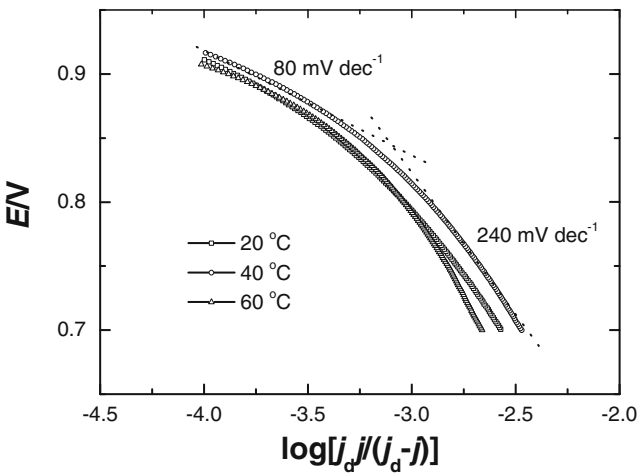

Fig. 6 Dependence of Tafel diagram for a H_I-ePt microelectrode/Nafion membrane equilibrated with O_2-saturated water on reaction temperature with data taken from the negative-going voltammograms in Fig. 4

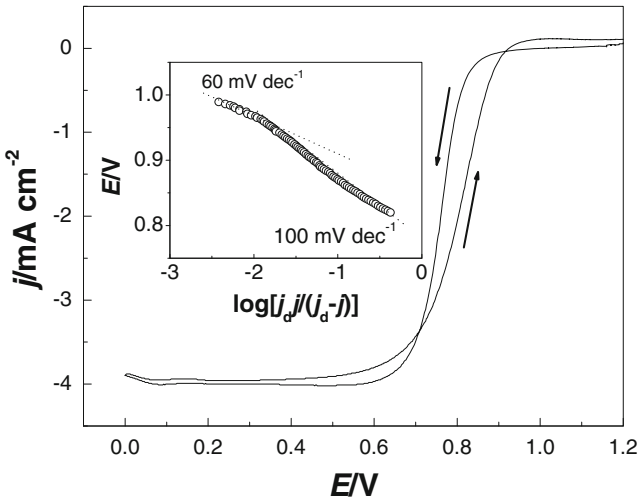

Fig. 7 Steady-state voltammograms for a H_I-ePt microelectrode in O_2-saturated 0.5 mol dm^{-3} H_2SO_4 (dE/dt, 5 mV s^{-1}). *Inset* Tafel plot obtained from the negatively going voltammogram

A value of the exchange current density (j_o) can be obtained by extrapolating the Tafel line to the equilibrium potential, E_{eq}, for the orr. In order to improve the accuracy of j_o, the equilibrium oxygen electrode potential at a given temperature should be determined. The dependence of E_{eq} on temperature was evaluated using the following equations [39]:

$$\Delta G^o = -295317 - 33.44T \ln T + 388.07T \tag{9}$$

$$E_{eq} = -\Delta G^o / nF \tag{10}$$

where ΔG^o is the free energy in joule per mole for the hydrogen and oxygen reaction producing liquid water and n is the number of electron transferred to produce one mole of water. The values of E_{eq} for the orr at 20, 40, and 60 °C are 1.229, 1.214, and 1.196 V vs. RHE, respectively. The values of j_o calculated from the real electrochemical surface area at each temperature are listed in Table 2. At low overpotentials, the orr is considered to proceed on a Pt oxide-covered surface [21]. The kinetics of the orr in the potential range relevant to fuel cell operation is considerably improved by increasing temperature. In comparison to literature data ranging from 10^{-11} to 10^{-9} A cm^{-2} [20, 21, 23, 24], the higher values of j_o in our condition suggest that the nanoporous Pt may be a class of potential electrocatalyst towards the orr. The activation energy for the orr at the Pt oxide-covered surface is about 58.0±0.4 kJ mol^{-1}. This value is very close to a reported value of 54.7 kJ mol^{-1} for the orr at the Pt/Nafion interface in the humidified condition and slightly smaller than the values of 73.2 [39] or 75.3 kJ mol^{-1} [12] reported by Parthasarathy et al. In a high overpotential region where the orr is most likely to occur at oxide-free Pt surfaces,

Table 2 Tafel slopes (b), exchange current density (j_o), and activation energy for the orr at a H_I-ePt microelectrode/Nafion membrane interface at a function of temperature

Temperature/K	Low current density		High current density
	b/V dec^{-1}	j_o/A cm^{-2}	b/V dec^{-1}
293	0.078	1.2×10^{-9}	0.232
313	0.085	5.6×10^{-9}	0.241
333	0.097	2.1×10^{-8}	0.300
E_a/kJ mol^{-1}	–	58.0±0.4	–

the j_o values may be distorted by the unusual Tafel slopes. Therefore, they are not provided in Table 2.

Discussion

It is of interest to discuss the polarization behavior of the nanoporous H_I-ePt on the Nafion membrane surface. The polarization theories of a porous electrode based on a simple pore model are used for our discussion since the pores inside the H_I-ePt electrode are highly ordered and less interconnected. Under activation–concentration overpotential control, the total current density can be expressed by [41]

$$j = \frac{\pi\gamma^2 DnFc^o}{l}[1-\exp(-\frac{F\eta}{RF})]K\tanh K \quad (11)$$

where

$$K^2 = \frac{2j_o l^2}{DnFc^o}\exp(\frac{F\eta}{2RT}) \quad (12)$$

where γ is the pore radius, l is the pore length, η is the overpotential, and other terms have their normal meanings. At high values of K, the Tafel slope will be $2RT/\beta F$, which is twice the normal value of the Tafel slope observed for planar electrode. When K assumes small values, i.e., at low values of j_o, η and at high values of the product $DnFc^o$, the current density in the pore is uniform and Tafel slope is given by $RT/\beta F$ as observed on planar electrodes for rate-determining discharge-type reactions. Under diffusion-controlled conditions, the limiting current appears.

The following noteworthy features are obtained under activation–Ohmic overpotential control [41]. At low η values and for low j_o, uniform current density distributed is expected and the Tafel slope is $RT/\beta F$. At high η values and for low ρ and γ, the current density distribution is non-uniform and the Tafel slope is $2RT/\beta F$, which is drawn from the following current–potential relationship:

$$\eta = \frac{2RT}{\beta nF}\ln j - \frac{2RT}{\beta nF}\ln(\frac{8j_o RT\rho\pi^2\gamma^2}{F})^{1/2} \quad (13)$$

where β is the symmetry factor, ρ is the specific conductance of the electrolyte, and other terms have their corresponding meanings described as above.

Figure 8 shows a single-pore model for the the H_I-ePt electrode on the Nafion membrane and in aqueous sulfuric acid solution. At the nanoporous Pt and Nafion membrane interface, all the current is mainly generated in the interface vicinity for both activation–concentration overpotential control and activation–Ohmic overpotential control since the transports of dissolved oxygen and ion charge carriers to the electrode are dominantly confined in the membrane. It is generally accepted that there are no mobile acids on the Nafion membrane surface and inside the membrane bulk owing to the fixing of ionic groups onto the membrane chains. If the orr occurs only at the contact interface between the electrode and the membrane or the polarization of the high surface area H_I-ePt electrode is homogeneous, a Tafel slope of 120 mV dec^{-1} would be obtained which is similar to that observed at a planar Pt electrode. However, this is different from the Tafel slope of around 240 mv dec^{-1} shown in Fig. 6. The double Tafel slope is a signature of the non-uniform polarization of the H_I-ePt electrode for the orr. The origins of this non-uniform polarization may be related to the contribution of the orr occurring at the reaction zones away from the membrane surfaces. It is reported that the electrochemical reaction zones can extend over the electrode and ionic membrane interface to the zones which are in no contact with the ionic membrane via the spillover of surface species without the need of adding supporting electrolyte [42, 43]. In our case, the orr is likely to occur at the nanoporous surfaces of the H_I-ePt electrode away from the membrane. However, high Ohmic overpotential will be expected since the nanopores away from the membrane are not filled with mobile acids. This high Ohmic potential results in the non-uniform electrode polarization characterized by a double Tafel slope. This explanation is supported by the change of the Tafel slope from around 240 mV dec^{-1} to around 100 mV dec^{-1} when the H_I-ePt electrode is moved away from the membrane surface into the O_2-saturated

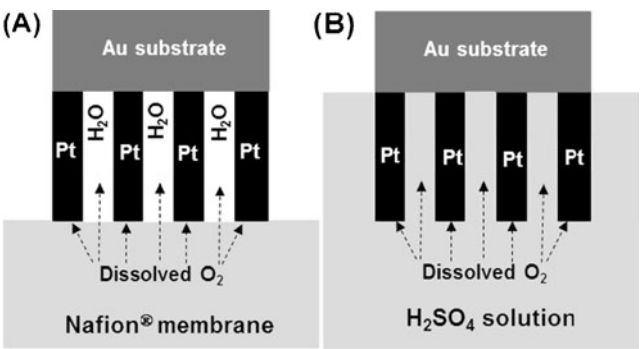

Fig. 8 A single-pore model for a H_I-ePt on Nafion membrane (**a**) and in 0.5 mol dm^{-3} H_2SO_4 solution (**b**)

0.5 mol dm^{-3} H_2SO_4 solution as shown in Fig. 7. In the acidic solution, the conductive solution can fill in the nanopores of the H_I-ePt electrode, leading to a considerable decrease in specific electrolyte resistance and Ohmic overpotential. The normal Tafel slope observed at the H_I-ePt electrode in sulfuric acid solution suggests that the electrode polarization is homogenous in the aqueous media with high electrolyte conductance and the H_I-ePt electrode could be considered as a planar electrode with highly developed surfaces.

The polarization behaviors of the H_I-ePt electrode in acidic solution and on the membrane strongly indicate that increasing electrolyte conductance inside a nanoporous electrode is important and efficient to achieve the homogeneous electrode polarization. This strategy has been used in a polymer electrolyte membrane fuel cell to increase the homogeneity of the electrode polarization by impregnating the electrode with a polymer electrolyte solution.

At the nanoporous Pt and Nafion membrane interface, dissolved oxygen could diffuse into the nanopores of the electrode from the Nafion membrane, following a similar diffusion pathway as the oxygen diffusion from the bulk solution to the electrode surface in the acidic solution, as shown in Fig. 8. If the activation–concentration polarization control is applied to the electrode on the membrane and in the aqueous solution, the double Tafel slope should be observed in both Figs. 6 and 7. However, this is not supported by the experimental results which show considerable change of the Tafel slope from 100 mV dec^{-1} to around 240 mV dec^{-1} when the electrode is moved away from the acidic solution onto the membrane surface. It is therefore reasonably considered that the double Tafel slope observed in Fig. 6 is less likely to be caused by the contribution of the activation–concentration overpotential control, compared to the activation–Ohmic overpotential control.

Conclusions

The solid polymer electrolyte composite nanostructured microelectrode constructed by mechanically pressing the nanoporous microelectrode onto the solid electrolyte membrane avoids the requirement of adding supporting electrolyte and can therefore be efficiently used to study the interfacial electrode kinetics and the activity of nanostructured electrocatalysts. It can serve as an in situ probe of the PEMFC reactions and electrocatalysis.

Measured higher exchange current densities for the orr at the interface between the nanoporous Pt electrode and Nafion membrane are indicative of improve reaction kinetics, as compared with literature results obtained in aqueous solution and at the polycrystalline Pt–Nafion interface. The orr at the nanoporous Pt and Nafion interface produces a two-section Tafel diagram exhibiting an abnormal slope at high overpotentials of doubling those obtained in acidic media and at the polycrystalline Pt–Nafion membrane interface. This abnormal Tafel slop suggests that the polarization of the nanoporous Pt electrode on the Nafion membrane is non-uniform. The origins of the non-uniform polarization could be related to the orr occurring at electrode surfaces away from the membrane with high Ohmic polarization.

References

1. Meza D, Morales U, Roquero P, Salgado L (2010) Inter J Hydrogen Energy 35:12111–12114
2. Takahashi I, Kocha S (2010) J Power Sources 195:6312–6322
3. Rao C, Viswanathan B (2010) J Phys Chem C 114:8661–8667
4. Jiang J, Rajagopalan K (2011) Electrochim Acta 46:717–722
5. Murthi V, Urian R, Mukerjee S (2004) J Phys Chem B 108:11011–11023
6. Raghuveer V, Manthiram A, Bard A (2005) J Phys Chem B 109:22909–22912
7. Toda T, Igarashi H, Uchida H, Watanabe M (1999) J Electrochem Soc 146:3750–3756
8. Yano H, Jung M, Uchida H, Watanabe M (2008) J Phys Chem C 112:8372–8380
9. Zhang J, Mo Y, Vukmirovic M, Klie R, Sasaki K, Adzic R (2004) J Phys Chem B 108:10955–10964
10. Xu Y, Ruban A, Mavrikakis M (2004) J Am Chem Soc 126:4717–4725
11. Wilson M, Goffesfeld S (1992) J Electrochem Soc 139:L28–L30
12. Parthasarathy A, Srinivasan S, Appleby A, Martin C (1992) J Electroanal Chem 339:101–121
13. Richards R, Bönnemann H (2001) Fuel Cells Bull 4:7–10
14. Poirier J, Stoner G (1994) J Electrochem Soc 141:425–430
15. Peuckert M, Yoneda T, Betta R, Boudart M (1986) J Electrochem Soc 113:944–947
16. Paulus U, Schmit T, Gasteiger H, Behm R (2001) J Electroanal Chem 495:134–145
17. Antoine O, Bultel Y, Durand R (2001) J Electroanal Chem 499:85–94
18. Gottesfeld S, Raistrick I, Srinivasan S (1987) J Electrochem Soc 134:1455–1462
19. Floriano J, Ticianelli E, Gonzalez E (1994) J Electroanal Chem 367:157–164
20. Parthasarathy A, Davé B, Srinivasan S, Appleby A, Martin C (1992) J Electrochem Soc 139:1634–1641
21. Parthasarathy A, Martin C, Srinivasan S (1991) J Electrochem Soc 138:916–921
22. Jiang J, Wu B, Cha C (1996) J Electroanal Chem 417:89–93
23. Basura V, Beattie P, Holdcroft S (1998) J Electroanal Chem 458:1–5
24. Beattie P, Basura V, Holdcroft S (1999) J Electroanal Chem 468:180–192
25. Jiang J, Wu B, Cha C (1998) J Electroanal Chem 446:159–163
26. Jiang J, Wu B, Cha C, Zhai R (1998) Electroanalysis 10:343–346
27. Jiang J, Kucernak A (2004) J Electroanal Chem 567:123–137
28. Jiang J, Kucernak A (2002) J Electroanal Chem 533:153–165
29. Jiang J, Kucernak A (2002) J Electroanal Chem 520:64–70
30. Evans S, Elliott J, Andrews L, Bartlett P, Doyle P, Denuault G (2002) Anal Chem 74:1322–1326
31. Nelson P, Owen J (2003) J Electrochem Soc 150:A1313–A1317
32. Koryta J, Dvořák J, Kavan L (1993) Principles of electrochemistry, 2nd edn. Wiley, Chichester

33. Denuault G, Mirkin M, Bard A (1991) J Electroanal Chem 308:27–38
34. Stutts K, Wightman R, Mark R (1983) Anal Chem 55:1576–1579
35. Verbrugge M (1989) J Electrochem Soc 136:417–423
36. Cha C, Li C, Yang H, Liu P (1994) J Electroanal Chem 368:47–54
37. Ogumi Z, Kuroe T, Takehara Z (1985) J Electrochem Soc 132:2601–2605
38. Ogumi Z, Takehara Z, Yoshizawa S (1984) J Electrochem Soc 131:769–773
39. Parthasarathy A, Srinivasan S, Appleby A, Martin C (1992) J Electrochem Soc 139:2530–2537
40. Lide D (1995) CRC handbook of chemistry and physics, 76th edn. CRC Press, London
41. Bockris J, Conway B, Yeager E (1981) Comprehensive treaties of electrochemistry, vol 3. Plenum, London
42. Tu W, Liu W, Cha C, Wu B (1998) Electrochim Acta 43:3731–3739
43. McBreen J (1985) J Electrochem Soc 132:1112–1116